Title

Evaluation of multi-color genetically encoded Ca2+ indicators in filamentous fungi

Authors

Kim, Hye-Seon
Kim, Jung-Eun
Hwangbo, Aram
et al.

Publication Date

2021-04-01

DOI

10.1016/j.fgb.2021.103540

Peer reviewed

Fungal Genetics and Biology 149 (2021) 103540

Contents lists available at ScienceDirect

Fungal Genetics and Biology

journal homepage: www.elsevier.com/locate/yfgbi

Tools and techniques

Evaluation of multi-color genetically encoded Ca^{2+} indicators in filamentous fungi

Hye-Seon Kim [a,b,1,2], Jung-Eun Kim [c,1,3], Aram Hwangbo [d], Jasper Akerboom [e,4], Loren L. Looger [e], Randall Duncan [a], Hokyoung Son [d], Kirk J. Czymmek [a,b,f,*], Seogchan Kang [c,*]

[a] Department of Biological Sciences, University of Delaware, Newark, DE 19716, United States
[b] Delaware Biotechnology Institute, Newark, DE 19711, United States
[c] Department of Plant Pathology & Environmental Microbiology, The Pennsylvania State University, University Park, PA 16802, United States
[d] Department of Agricultural Biotechnology, Seoul National University, Seoul 151-921, Republic of Korea
[e] Janelia Research Campus, Howard Hughes Medical Institute, Ashburn, VA 20147, United States
[f] Donald Danforth Plant Science Center, Saint Louis, MO 63132, United States

ARTICLE INFO

Keywords:
Calcium signature
Fusarium
Genetically encoded calcium indicators
Signaling
Time-lapse imaging

ABSTRACT

Genetically encoded Ca^{2+} indicators (GECIs) enable long-term monitoring of cellular and subcellular dynamics of this second messenger in response to environmental and developmental cues without relying on exogenous dyes. Continued development and optimization in GECIs, combined with advances in gene manipulation, offer new opportunities for investigating the mechanism of Ca^{2+} signaling in fungi, ranging from documenting Ca^{2+} signatures under diverse conditions and genetic backgrounds to evaluating how changes in Ca^{2+} signature impact calcium-binding proteins and subsequent cellular changes. Here, we attempted to express multi-color (green, yellow, blue, cyan, and red) circularly permuted fluorescent protein (FP)-based Ca^{2+} indicators driven by multiple fungal promoters in *Fusarium oxysporum*, *F. graminearum*, and *Neurospora crassa*. Several variants were successfully expressed, with GCaMP5G driven by the *Magnaporthe oryzae* ribosomal protein 27 and *F. verticillioides* elongation factor-1α gene promoters being optimal for *F. graminearum* and *F. oxysporum*, respectively. Transformants expressing GCaMP5G were compared with those expressing YC3.60, a ratiometric Cameleon Ca^{2+} indicator. Wild-type and three Ca^{2+} signaling mutants of *F. graminearum* expressing GCaMP5G exhibited improved signal-to-noise and increased temporal and spatial resolution and are also more amenable to studies involving multiple FPs compared to strains expressing YC3.60.

1. Introduction

A network of signaling pathways coordinates organismal responses to external stimuli to ensure short-term cellular homeostasis and direct orderly long-term growth and development. Among the second messengers that function to regulate and link various signaling pathways, Ca^{2+} is probably the most versatile and regulates a plethora of cellular and developmental processes in microbes, animals, and plants (Hofer and Brown, 2003; Slusarski and Pelegri, 2007; Steinhorst and Kudla, 2014). Extracellular stimuli create specific spatial and temporal distribution patterns of cytoplasmic Ca^{2+} ($[Ca^{2+}]_c$), referred to as the Ca^{2+} "signature", via influxes and effluxes of Ca^{2+} to and from the extracellular environment and internal Ca^{2+} stores through the action of ion channels, pumps, and transporters on plasma and organellar membranes (Crichton, 2012; McAinsh and Pittman, 2009). The Ca^{2+} signature modulates the cellular localization or activity of diverse Ca^{2+}-binding proteins (CBPs) and CBP-interacting proteins. The resulting cascades of molecular changes and interactions drive specific cellular responses

* Corresponding authors at: Advanced Bioimaging Laboratory, Donald Danforth Plant Science Center, Saint Louis, MO 63132, United States (K.J. Czymmek) and Department of Plant Pathology & Environmental Microbiology, The Pennsylvania State University, University Park, PA 16802, United States (S. Kang).
E-mail addresses: kczymmek@danforthcenter.org (K.J. Czymmek), sxk55@psu.edu (S. Kang).
[1] These authors contributed equally.
[2] Current address: USDA, Agricultural Research Service, National Center for Agricultural Utilization Research, Mycotoxin Prevention and Applied Microbiology Research Unit, 1815 N. University, Peoria, IL. 61604, United States.
[3] Current address: Research Institute Agriculture and Life Science, Seoul National University, Seoul 151-921, Republic of Korea.
[4] Current address: Jasper Yeast, Dulles, VA 20166, United States.

https://doi.org/10.1016/j.fgb.2021.103540
Received 21 August 2020; Received in revised form 27 January 2021; Accepted 30 January 2021
Available online 16 February 2021

(Clapham, 2007; Dodd et al., 2010). Accordingly, to understand the mechanism of Ca^{2+} signaling, studying how Ca^{2+} signatures form in response to different stimuli and under different environmental conditions is crucial.

Initial attempts to image the Ca^{2+} signature in fungi employed ratiometric chemical indicators that change their spectral properties upon Ca^{2+} binding, such as Indo-1, Fluo-4 with Cell Trace Calcein Red-Orange-AM, and Fura-2 (Nair et al., 2011; Silverman-Gavrila and Lew, 2003). While highly sensitive to Ca^{2+}, these indicators have notable limitations, including difficulties in intracellular loading, leakage, rapid conversion of the indicators to membrane-impermeable forms by cell wall esterases, and sequestration within non-targeted organelles. They also are unsuitable for long-duration, time-lapse imaging experiments due to their short *in vivo* lifetime (Paredes et al., 2008). Diverse genetically encoded Ca^{2+} indicators (GECIs), developed primarily to enable the visualization and quantification of transient changes of $[Ca^{2+}]_c$ in animal cells (Demaurex, 2005; Grienberger and Konnerth, 2012; Kanchiswamy et al., 2014; Takahashi et al., 1999; Thomas et al., 2000), helped overcome these limitations. Aequorin is a naturally evolved, bioluminescent GECI produced by *Aequorea victoria* photocytes (wherein it provides the natural excitation light for Green Fluorescent Protein, GFP) and was successfully expressed in filamentous fungi (Knight et al., 1991; Martin et al., 2007; Nelson et al., 2004). However, due to its low signal, aequorin is not suitable for imaging $[Ca^{2+}]_c$ dynamics in individual cells and has been primarily used to quantify collective $[Ca^{2+}]_c$ changes in cell populations. Furthermore, its requirement of the exogenous substrate coelenterazine hampers usage. GECIs based on GFP and other fluorescent proteins (FPs) offer multiple advantages: they are bright and photostable, require no small molecule addition for fluorescence, have an excellent signal change, and can be targeted to specific organelles (Borst et al., 2008; Demaurex, 2005; Nagai et al., 2004). GECIs have enabled visualization of Ca^{2+} dynamics in plant and animal cells over time (Hasan et al., 2004; Horikawa et al., 2010; Monshausen et al., 2008; Rudolf et al., 2004; Watahiki et al., 2004). Such indicators typically consist of a Ca^{2+} binding protein, such as troponin C or a combination of calmodulin (CaM) and the myosin light-chain kinase M13 peptide, fused to one or two FPs. They reversibly change their spectral properties, either brightness of a single, circularly permuted FP or Förster resonance energy transfer (FRET) between two FPs, through association/disassociation with Ca^{2+} (Kotlikoff, 2007; Liu et al., 2011; McCombs and Palmer, 2008).

The Cameleon family of FRET GECIs has been used to study $[Ca^{2+}]_c$ in animals and plants (Diegelmann et al., 2002; Hasan et al., 2004; Krebs et al., 2012; Miwa et al., 2006; Rincón-Zachary et al., 2010). We reported the first successful expression of Yellow Cameleon YC3.60 in filamentous fungi (Kim et al., 2012), which allowed the visualization over time of Ca^{2+} signatures in hyphal tips as they grew on different media and interacted with plants. This success also allowed us to study how individual or combinations of genes involved in Ca^{2+} signaling contribute to the formation of Ca^{2+} signature via mutagenesis of these genes in *Fusarium oxysporum* (Kim et al., 2015) and *F. graminearum* (Kim et al., 2018). However, imaging with YC3.60 has several shortcomings: it has a relatively limited dynamic range and slow kinetics, and FRET indicators occupy a large portion of the visible spectrum. GECIs with faster kinetics, larger signal change, and wider dynamic range of $[Ca^{2+}]$ detection are needed to enable more experiments. In particular, single-FP GECIs occupy less spectral bandwidth than FRET-based GECIs, allowing simultaneous multi-color imaging.

Advances in protein engineering have expedited the development of GECIs with specific characteristics for different purposes (Akerboom et al., 2013, 2012). Camgaroo (Baird et al., 1999), a single-FP GECI, was used to produce the original GCaMP – a fusion of GFP, CaM, and the M13/RS20 CaM-binding peptide (Akerboom et al., 2013, 2012; Nakai et al., 2001; Tian et al., 2009). The original scaffold of GCaMP has been iteratively improved by several labs over the last 20 years (Kostyuk et al., 2019), resulting in GCaMP2 (Nagai et al., 2004), GCaMP3 (Akerboom et al., 2013, 2012; Nakai et al., 2001; Tian et al., 2009), GCaMP5 (Akerboom et al., 2013, 2012; Nakai et al., 2001; Tian et al., 2009), GCaMP6 (Chen et al., 2013), and jGCaMP7 (Dana et al., 2019). Other color variants, particularly red sensors, have also been developed. Available red GECIs include RCaMP (Akerboom et al., 2013, 2012), RGECO1 (Zhao et al., 2011), and their improved variants jRCaMP1 and jRGECO1a (Dana et al., 2016). GCaMP indicators detected local Ca^{2+} changes in very small structures thanks to increased brightness and reduced Ca^{2+} buffering capacity compared to other Ca^{2+} indicators (Ohkura et al., 2005).

In this study, we evaluated if a group of multi-color, circularly permuted FP-based GECIs developed for imaging neural activity (Akerboom et al., 2013, 2012) could be expressed in three fungal species for subcellular time-lapse imaging of Ca^{2+} dynamics.

2. Materials and methods

2.1. Strains and growth conditions

Fusarium graminearum strain GZ03639 (Bowden and Leslie, 1999) and *F. oxysporum* f.sp. *lycopersici* strain Fol4287 (Ma et al., 2010) were stored as a conidial suspension in 20% glycerol at −80 °C. Potato dextrose agar (PDA; Difco, Sparks, MD) was used to activate these strains for experiments. Macroconidia of *F. graminearum* and microconidia of *F. oxysporum* were produced by culturing them in carboxymethyl cellulose (CMC) medium (Kim et al., 2012) at 25 °C for 7 days with vigorous shaking. *Neurospora crassa* strain FGSC 2489 (Galagan et al., 2003), which was preserved on silica gel at −20 °C, was cultured on Vogel's N medium (Davis and de Serres, 1970). Genomic DNA was extracted from mycelia cultured in potato dextrose broth (HiMedia, India) at 25 °C for 5 days. *Escherichia coli* strains DH5α and XL1Blue were used for building and maintaining vector constructs.

2.2. Construction of vectors carrying GECIs driven by multiple fungal promoters

The primers used for vector construction are listed in Supplementary Table 1. The GECIs evaluated include two GCaMPs (GCaMP3 and GCaMP5G), five RCaMPs (RCaMP1d, RCaMP1e, RCaMP1f, RCaMP1g, and RCaMP1h), two YCaMPs (YCaMP1a and YCaMP1b), two CyCaMPs (CyCaMP1a and CyCaMP1b), and two BCaMPs (BCaMP1a and BCaMP1b) (Akerboom et al., 2013). The open reading frames (ORFs) of these GECIs (1.2–1.3 kb), except that of RCaMP1d, were amplified by PCR using primers GCaMP-F and CaMP-R, which contain *Bam*HI and *Sph*I restriction sites, respectively, at the 5′ end to facilitate subsequent cloning under multiple promoters. The ORF of RCaMP1d was amplified using primers RCaMP1d-F, containing *Bam*HI site at the 5′ end, and CaMP-R. Amplified ORFs were cloned into pGEM-T Easy (Promega, Madison, WI) and sequenced to confirm that PCR did not cause sequence changes.

Each ORF, released using *Bam*HI and *Sph*I, was cloned under several fungal promoters (Supplementary Fig. 1). For cloning these ORFs between the *Cochliobolus heterostrophus* glyceraldehyde-3-phosphate dehydrogenase gene promoter (P_{GAPD}) and the *N. crassa* β-tubulin gene terminator ($T_{β\text{-tubulin}}$), pSK1732, a vector that carries the EGFP ORF between P_{GAPD} and $T_{β\text{-tubulin}}$ in pGEM-3Zf (Promega, Madison, WI), was used. We replaced the EGFP ORF in pSK1732 with each GECI ORF. Individual GECI ORFs were also ligated between the *M. oryzae* ribosomal protein 27 gene promoter (P_{RP27}) and $T_{β\text{-tubulin}}$ in pSK1736. The 670-bp *F. verticillioides* elongation factor-1α gene promoter ($P_{EF1α}$) was released from pSK2325 (Kim et al., 2012) using *Eco*RI and *Bam*HI. This fragment was inserted into *Eco*RI-*Bam*HI digested pRP27-GCaMP3 (P_{RP27}::C_{GCaMP3}::$T_{β\text{-tubulin}}$) to construct $P_{EF1α}$::C_{GCaMP3}::$T_{β\text{-tubulin}}$. Vectors carrying other GECIs driven by $P_{EF1α}$ were generated using the strategy employed for pEF1α-GCaMP3 construction. For expression of GCaMP3, GCaMP5G, RCaMP1d, and RCaMP1e in *N. crassa*, the *N. crassa ccg-1*

gene promoter (P_{CCG1}) was amplified from pAL3-Lifeact (Berepiki et al., 2010), which was provided by Dr. Nick Read at the University of Manchester, using primers CCG1p-F_EcoRI and CCG1p-R. The amplified P_{CCG1} was cloned into pGEM-T Easy vector for sequence verification. The P_{CCG1}, released via *Eco*RI and *Bam*HI digestion, was ligated into *Eco*RI and *Bam*HI digested pRP27-GCaMP3, pRP27-GCaMP5G, pRP27-RCaMP1d, and pRP27-RCaMP1e. All constructs generated in this study are noted in Supplementary Table 2.

2.3. Generation and screening of fungal transformants

Each GECI construct and a gene conferring resistance to hygromycin B or geneticin were introduced to individual fungi using a polyethylene glycol (PEG)-mediated transformation protocol (Son et al., 2011). The amount of lysing enzymes and the digestion time to generate protoplasts varied among *N. crassa*, *F. graminearum*, and *F. oxysporum*. We monitored the progression of protoplast formation using a hemocytometer and microscope.

Transformants of *F. graminearum* were generated by mixing protoplasts with each GECI construct, linearized using a restriction enzyme *Nae*I or *Eco*RI, and a construct harboring the geneticin resistance gene (Lee et al., 2010). Twenty-four geneticin-resistant transformants with each construct were screened via PCR with primers CaMP-scrF (5′-CATCACGTCGTAAGTGGAATAAGAC-3′) and CaMP-scrR (5′-CTCTGCTTCTGTGGGGTTCTG-3′). These primers were designed to anneal to the conserved parts of all GECI ORFs. We checked fluorescence of 10 randomly chosen PCR-positive transformants using a fluorescence microscope (Leica DM6 B, Germany). For *N. crassa* and *F. oxysporum*, we skipped PCR and directly screened 20–50 randomly selected transformants with each construct using a fluorescence microscope (Zeiss Axiovert 200, Germany). The hygromycin B and geneticin resistance genes used for cotransformation of *N. crassa* and *F. oxysporum* were amplified from pSK2978 (primers Gen-For and PLC24-gfpR) and pII99 (primers Gen-For and Gen-Rev), respectively. We screened 3–5 transformants per construct using a Zeiss LSM780 imaging system to determine whether their fluorescence intensity and stability was suitable for time-lapse imaging of $[Ca^{2+}]_c$ dynamics (performed as described in 2.5).

2.4. Mutagenesis of F. graminearum strain GZ03639 expressing GCaMP5G

Strain FSK719, a geneticin-resistant transformant of GZ03639 with pRP27-GCaMP5G, was chosen for disrupting the *CCH1*, *MID1*, and *FIG1* genes. Colony growth, conidiation, sexual development, trichothecene production, and virulence on wheat plants of FSK719 and GZ03639 were measured as described in our previous study (Kim et al., 2018) to ensure that the transformation process and the expression of GCaMP5G did not affect GZ03639. The mutant alleles for *CCH1*, *MID1*, and *FIG1* were constructed using a split marker strategy as previously described (Kim et al., 2018) with the hygromycin B resistance gene as a selection marker. Each mutant allele was introduced into protoplasts of FSK719. All mutants were confirmed using PCR and Southern analysis.

2.5. Microscopy and data analyses

After inoculating 1 μl of 5×10^5/ml spore suspension at the bottom of μ-dish 50 mm-low Ibidi chamber or μ-slide 8 well with uncoated #1.5 Ibidi polymer coverslip (Ibidi, Fitchburg, WI) containing PDA or Vogel's medium supplemented with 1 mM $CaCl_2$, they were incubated at 26 °C with minimal light (Kim et al., 2015). For consistency, hyphal tip $[Ca^{2+}]_c$ imaging was performed 2 days post inoculation. Three leading hyphal tips for each strain were imaged every 1.84 s for at least 20–30 min with three replicates.

For imaging $[Ca^{2+}]_c$ changes in response to chemical treatment, two days old hyphal tips in μ-slide 8 well were imaged for several minutes to establish the baseline. After applying 40 μM of 4-Bromo A-23187 (Thermo Fisher Scientific, Waltham, WA), a Ca^{2+} ionophore, in 1 mM $CaCl_2$ solution, the same hyphal tips were imaged for 30–60 min. A Zeiss LSM 5 DUO or Zeiss LSM 780 laser scanning confocal microscope with 40x oil Plan-Neofluor (1.3 numerical aperture) oil immersion objective lens was used for imaging. Ratiometric imaging of $[Ca^{2+}]_c$ was performed for strains expressing Cameleon YC3.60. LSM 510 AIM software (Rel. 4.2) was used for ratiometric data processing. The 458 nm laser line of a 25 mW argon ion laser was used to acquire data via three channels (YFP, CFP, and transmitted light). Corresponding YFP/CFP ratio images with background subtraction were acquired as previously described (Kim et al., 2015, 2012). For $[Ca^{2+}]_c$ imaging based on GCaMP, YCaMP, RCaMP, BCaMP, and CyCaMP, a Zeiss LSM780 (ZEN 2009) imaging system equipped with the following filter sets was used: (a) GCaMP with a laser excitation of 488 nm, Filters: 490–560 nm, Beam Splitters-MBS 488 nm; (b) YCaMP with a laser excitation of 514 nm, Filters: 520–555 nm, Beam Splitters- MBS 488/514/561 nm; (c) RCaMP with a laser excitation of 560 nm, Filters: 575–615 nm, Beam Splitters-MBS 458/514/561 nm; (d) BCaMP with a laser excitation of 405 nm, Filters: 420–480 nm, Beam Splitters-MBS 405/488/561 nm; and (e) CyCaMP with a laser excitation of 458 nm, Filters: 465–510 nm, Beam Splitters-MBS 458 nm.

2.6. Analysis of Ca^{2+} signatures

We quantified the mean fluorescent intensity in a region of interest (ROI) of individual hyphal tip images in a time-lapse series (for both ratiometric or non-ratiometric indicators) using an ImageJ automated tip Tracking Macro (http://rsb.info.nih.gov/ij/), as previously described (Kim et al., 2015, 2012). The resulting images and plots were processed and generated using the ZEN 2009 software tool and ImageJ background subtraction.

3. Results

3.1. Evaluation of multiple circularly permuted FP-based GECIs with different spectral properties in three fungal species

To expand a toolbox for studying the spatial and temporal dynamics of Ca^{2+} signature and the mechanism underlying fungal Ca^{2+} signaling, we evaluated whether 13 GECIs developed for neural activity imaging (Akerboom et al., 2013, 2012) could function in *F. oxysporum*, *F. graminearum*, and *N. crassa*. The GECIs evaluated (Supplementary Table 2) included those based on green FP (GCaMP3 and GCaMP5G), red FP (RCaMP1d, RCaMP1e, RCaMP1f, RCaMP1g and RCaMP1h), blue FP (BCaMP1a and BCaMP1b), yellow FP (YCaMP1a and YCaMP1b), and cyan FP (CyCaMP1a and CyCaMP1b). We also tested four fungal gene promoters (Supplementary Fig. 1 and Supplementary Table 2), including the *C. heterostrophus* glyceraldehyde-3-phosphate dehydrogenase gene promoter (P_{GAPD}), the *M. oryzae* ribosomal protein 27 gene promoter (P_{RP27}), the *F. verticillioides* elongation factor-1α gene promoter ($P_{EF1\alpha}$) and the *N. crassa ccg-1* gene promoter (P_{CCG1}), to identify promoter(s) that work best in individual species.

Because the number of GECI constructs and transformants to be screened was very large, we did not transform all species with all constructs. Instead, we initially tested the expression of GCaMP3, GCaMP5G, RCaMP1d, and RCaMP1e driven by P_{GAPD}, P_{RP27} and $P_{EF1\alpha}$ (Supplementary Table 2) in *F. oxysporum*, *F. graminearum*, and *N. crassa*. Because we cotransformed these species with individual constructs with a gene conferring resistance to hygromycin B or geneticin as a selection marker, some transformants would only carry the hygromycin B or geneticin resistance gene. To evaluate the frequency of cotransformation, 24 randomly chosen transformants of *F. graminearum* with each of the 12 constructs were screened by PCR for the presence of GECI. More than 50% of the transformants were PCR positive. Ten PCR-positive transformants with each construct were screened using a fluorescence microscope (Supplementary Table 2). For *N. crassa* and *F. oxysporum*, we

directly screened 20–50 randomly selected transformants with each construct for fluorescence (20 in cases many transformants were fluorescent; up to 50 in cases none or only a very few were fluorescent) without performing PCR. Based on the initial evaluation using a regular fluorescent microscope, we screened 3–5 transformants per construct using a confocal microscope to determine whether their fluorescence intensity and stability was suitable for time-lapse imaging of $[Ca^{2+}]_c$ dynamics.

We could not detect discernable red fluorescence in any of the transformants containing any RCaMPs under all three promoters, with one exception (Supplementary Table 2). In one *F. graminearum* transformant, we noted that RCaMP1d was expressed but appeared aggregated (non-uniform distribution in the cytoplasm presumably due to aggregation or sequestration of the FP). Only GCaMP3 under $P_{EF1\alpha}$ was detectably expressed in *N. crassa*, but fluorescence was unstable. Accordingly, we also generated constructs with GCaMP3, GCaMP5G, RCaMP1d, and RCaMP1e under the control of P_{CCG1}, a promoter that has been commonly used for constitutively expressing proteins in *N. crassa*. However, none of the constructs generated detectable fluorescent signals or produced signals strong enough for time-lapse Ca^{2+} imaging. The *M. oryzae* RP27 promoter (P_{RP27}), which worked best in *F. graminearum*, was chosen to express the remaining GECIs in *F. graminearum*. Unfortunately, none of the RCaMPs produced a detectable fluorescence signal. BCaMP1b and CyCaMP1b were expressed, but not at the level that is suitable or responsive for time-lapse Ca^{2+} imaging. The other BcaMP and CyCaMP did not express at a detectable level. Only YCaMP1a exhibited brightness comparable to that of GCaMP5G. In *F. oxysporum*, we observed expression strong enough for Ca^{2+} imaging only with GCaMP5G under $P_{EF1\alpha}$. We introduced the remaining GECIs under $P_{EF1\alpha}$ into *F. oxysporum*, but fluorescence signals from all BCaMPs, CyCaMPs, and YCaMPs were not detectable or too weak. Thus, we focused our subsequent imaging and Ca^{2+} signature analysis on transformants with P_{RP27}-GCaMP5G and P_{RP27}-YCaMP1a for *F. graminearum*, $P_{EF1\alpha}$-GCaMP5G for *F. oxysporum*, and $P_{EF1\alpha}$-GCaMP3 for *N. crassa*. We chose transformants with colony growth rates comparable to untransformed parental strains. Assessment and confirmation of the cytoplasmic localization of Ca^{2+} in the selected strains showed a pattern with overall uniform distribution and single bright foci at actively growing hyphal tips (noted by arrows in Fig. 1A, B, E, I, and K) and best visualized in respective movies. The location of low intensity fluorescence foci with GCaMP5G variants matched to calmodulin localization at the Spitzenkörper core (Chen et al., 2010; Kim et al., 2012; Wang et al., 2006), but was very difficult to discern in YC3.60 (only yellow channel, Fig. 1E and respective movie) and never visible in the ratio image (Fig. 1G & H and 1G movie). The ability to simultaneously monitor the Spitzenkörper core in relation to Ca^{2+} dynamics via GCaMP5G provides an indication of the Spitzenkörper status and is beneficial for multi-label experiments.

3.2. Comparison of Ca^{2+} signatures in multiple species analyzed using spectral variants of GCaMP

Using the GECI variants expressed in individual species, we determined whether they could be used for imaging pulsatile Ca^{2+} signatures, similar to our previous work with YC3.60 (Kim et al., 2018, 2015, 2012). First, we analyzed Ca^{2+} signatures in *F. graminearum* using GCaMP5G and YCaMP1a driven by the promoter P_{RP27}. In general, both transformants grown for 2 days on Vogel's medium supplemented with 1 mM $CaCl_2$ showed excellent signal-to-noise (S/N) and exhibited conspicuous pulsatile signatures (Fig. 2A). However, with YCaMP1a, we noted an increased tendency of gradual photobleaching (~36% over 10 min

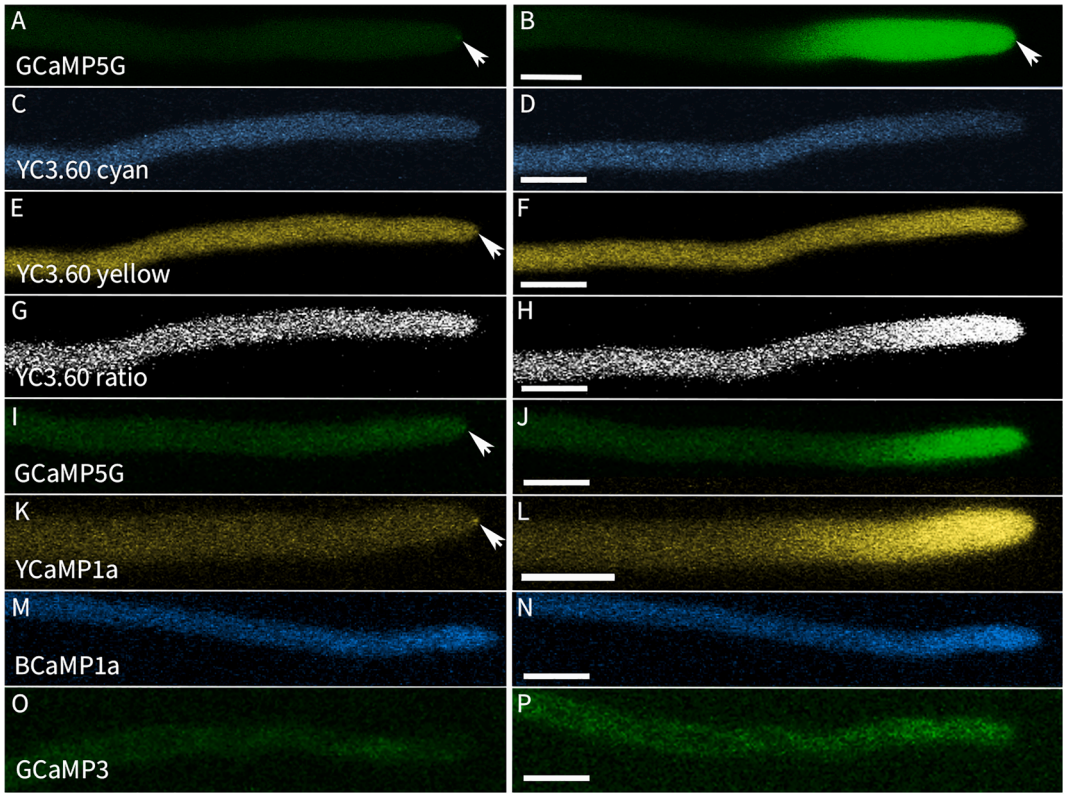

Fig. 1. Comparison of GECI localization at basal and peak $[Ca^{2+}]_c$ transients in hyphal tips of *F. graminearum*, *F. oxysporum* and *N. crassa*. The left and right columns show images corresponding to basal (non-gradient) and peak (gradient) $[Ca^{2+}]_c$ transients, respectively. *F. graminearum* expressing GCaMP5G (A and B), *F. graminearum* expressing YC3.60 - cyan channel (C and D), *F. graminearum* expressing YC3.60 - yellow channel (E and F), *F. graminearum* expressing YC3.60 – ratio (G and H), *F. oxysporum* expressing GCaMP5G (I and J), *F. graminearum* expressing YCaMP1a (K and L), *F. graminearum* expressing BCaMP1a (M and N), *N. crassa* expressing GCaMP3 (O and P). Arrowheads indicate Spitzenkörper affiliated calmodulin puncta when visible and confirmed in time-lapse movies. All samples were imaged after culturing on Vogel containing 1 mM $CaCl_2$ for 2 days at 25 °C. Scale bars = 10 μm.

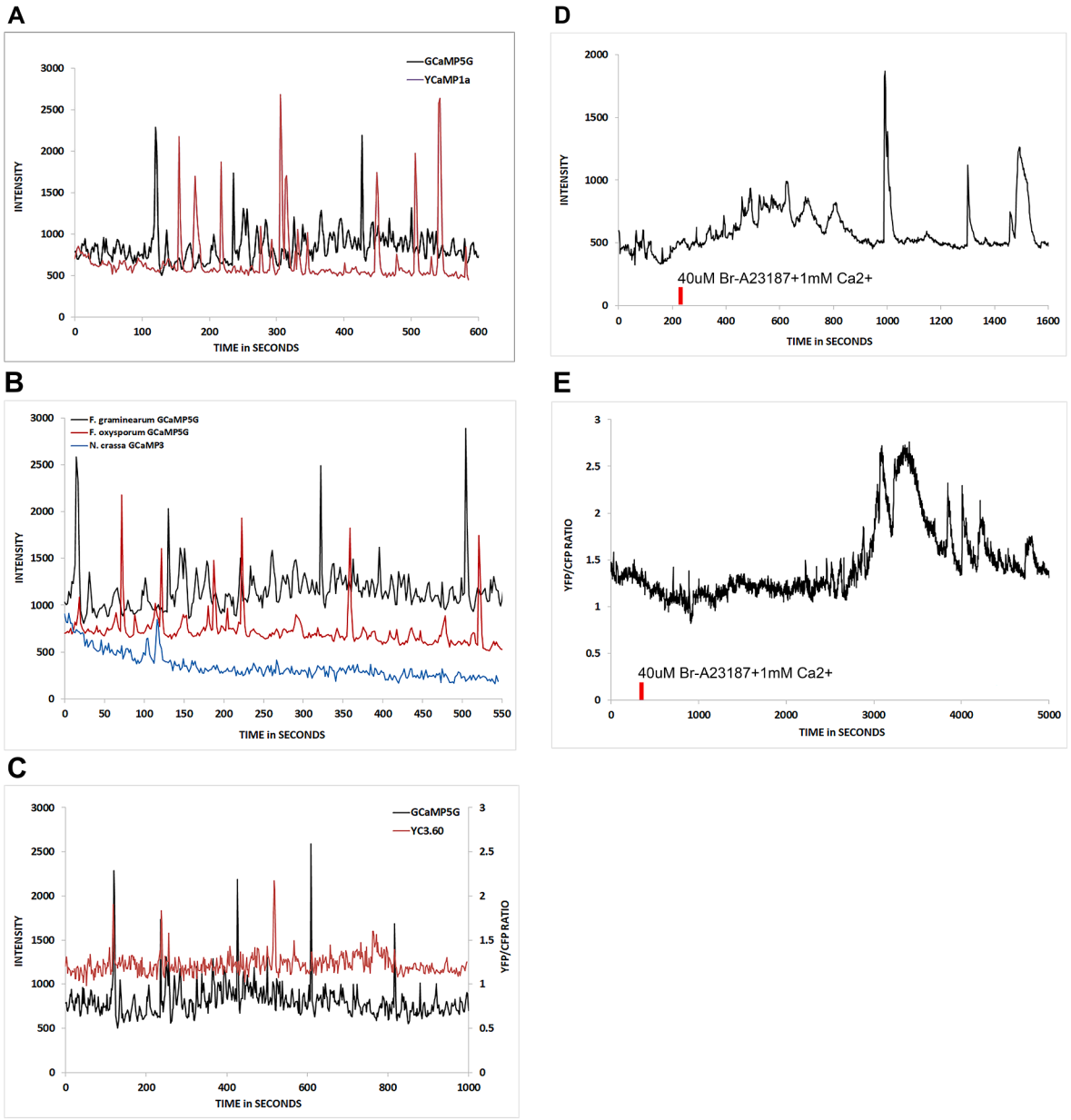

Fig. 2. Comparison of Ca^{2+} signatures imaged using different GECIs. (A) Ca^{2+} signatures in *F. graminearum* expressing YCaMP1a and GCaMP5G. Representative hyphal tips of *F. graminearum* strain GZ03639 transformed with pRP27-GCaMP5G (black line) and pRP27-YCaMP1a (red line) were imaged after culturing them on Vogel containing 1 mM $CaCl_2$ for 2 days at 25 °C. (B) Comparison of Ca^{2+} signatures in three fungal species expressing GCaMP. Hyphal tips of *F. graminearum* transformed with pRP27-GCaMP5G (black line), *F. oxysporum* transformed with pEF1α-GCaMP5G (red line), and *N. crassa* transformed with pEF1α-GCaMP3 (blue line) were imaged after culturing them on Vogel agar containing 1 mM $CaCl_2$ for 2 days at 25 °C. (C) Comparison of *F. graminearum* Ca^{2+} signatures analyzed using GCaMP5G and YC3.60. Hyphal tips of strain GZ03639 transformed with pRP27-GCaMP5G (black line) and YC3.60 (red line) imaged after culturing them on Vogel agar containing 1 mM $CaCl_2$ for 2 days at 25 °C. (D, E) Ca^{2+} signatures in *F. graminearum* in response to 4-Bromo A-23187, a Ca^{2+} ionophore. Hyphal tips of strain GZ03639 transformed with (D) pRP27-GCaMP5G and (E) YC3.60 cultured on PDA for 2 days at 25 °C were imaged before and after the application of 40 μM of 4-Bromo A-23187 in 1 mM $CaCl_2$ (noted by the red bar). (For interpretation of the references to color in this figure legend, the reader is referred to the web version of this article.)

continuous imaging) and more frequent large amplitude peaks (i.e., up to ~ 5X intensity change from basal cytoplasm levels; Fig. 2A, red line). We then analyzed Ca^{2+} signatures in *F. graminearum* carrying P_{RP27}-GCaMP5G, *F. oxysporum* transformed with $P_{EF1\alpha}$-GCaMP5G, and *N. crassa* carrying $P_{EF1\alpha}$-GCaMP3 (Fig. 2B). Both *F. graminearum* carrying P_{RP27}-GCaMP5G and *F. oxysporum* carrying $P_{EF1\alpha}$-GCaMP5G exhibited Ca^{2+} signatures that were high-quality and consistent with our prior data based on YC3.60 (compare Figs. 1A & 2A in Kim et al., 2015, with Fig. 2B red line). However, *N. crassa* containing $P_{EF1\alpha}$-GCaMP3, the only construct that produced detectable fluorescence signal in *N. crassa*, lacked consistent or intense Ca^{2+} signatures during time-lapse hyphal tip imaging. Additionally, photobleaching was severe, with the basal fluorescence signal decreasing nearly 51% in this 550-second representative series. Unfortunately, while some $[Ca^{2+}]_c$ transients could be documented, *N. crassa* with $P_{EF1\alpha}$-GCaMP3 was not suitable for meaningful long-term observations.

3.3. Comparison of the Ca^{2+} signatures imaged using GCaMP5G and YC3.60 under identical genetic backgrounds and culture conditions

We evaluated whether GCaMP5G exhibited tip high pulsatile Ca^{2+} signatures comparable to those observed using YC3.60. Time-lapse experiments (1,000 s) with *F. graminearum* expressing GCaMP5G showed representative Ca^{2+} signatures with repetitive low level Ca^{2+} oscillations every 10–30 s and occasional large amplitude spikes (Fig. 2C). While the overall pattern observed using GCaMP5G was quite similar to that based on YC3.60, notable differences were the increased amplitude of both small and large peaks and improved signal-to-noise ratio (black vs. red lines in Fig. 2C). These differences were partly due to the non-ratiometric FP design and the lack of fluorescence from GCaMP5G when unbound to Ca^{2+}, reducing overall background.

3.4. Comparison of GCaMP5G and YC3.60 via $[Ca^{2+}]_c$ response to a Ca^{2+}-selective ionophore

We tested if *F. graminearum* transformants expressing GCaMP5G and YC3.60 respond comparably to 4-Bromo A-23187, a non-fluorescent Ca^{2+}-selective ionophore. We noted experimental variability in initial $[Ca^{2+}]_c$ response following ionophore application (Fig. 2D & E, red bar), which was likely due to differences in diffusion and local concentration of the ionophore as it passed through the agar to the observed hyphal tip. Irrespective of onset delay, 4-Bromo A-23187 disrupted the periodic low amplitude Ca^{2+} signatures in both transformants. Instead, it caused a series of pronounced high-amplitude, closely spaced peaks with broad profiles lasting several minutes (Fig. 2D & E) and temporary cessation of hyphal tip growth. Upon treatment with 4-Bromo A-23187, GCaMP5G typically exhibited a ~ 4-fold change in signal intensity increase over basal levels (Fig. 2D) while YC3.60 exhibited a 2-fold ratio (Fig. 2E) maximal change over basal levels. Together, this data suggested that GCaMP5G and YC3.60 respond to 4-Bromo A-23187 as expected: the transient opening of Ca^{2+} channels results in a massive cytoplasmic Ca^{2+} influx, likely from both internal and external pools, and then $[Ca^{2+}]_c$ gradually returns to homeostasis.

3.5. Comparison of GCaMP5G and YC3.60 for imaging $[Ca^{2+}]_c$ changes in Ca^{2+} channel mutants of F. graminearum

Previously, we used YC3.60 to assess how disruption of Ca^{2+} channels affects Ca^{2+} signatures in *F oxysporum* (Kim et al., 2015) and *F. graminearum* (Kim et al., 2018). We tested the suitability of GCaMP5G for similar studies using *F. graminearum* mutants defective in three Ca^{2+} channel genes, including *CCH1* and *MID1*, which encode a high-affinity Ca^{2+} uptake system, and *FIG1*, a low-affinity Ca^{2+} channel. The *CCH1*, *MID1*, and *FIG1* genes in strain FSK719, a transformant of GZ03639 with pRP27-GCaMP5G, were disrupted via transformation-mediated gene replacement. No significant differences in colony growth, conidiation, sexual development, trichothecene production, and virulence were detected between FSK719 and GZ03639 (Supplementary Fig. 2), suggesting that the transformation process and the expression of GCaMP5G did not affect GZ03639. Analysis of Ca^{2+} signatures in the mutants Δ*mid1*, Δ*cch1*, and Δ*fig1* expressing either YC3.60 or GCaMP5G was performed (Fig. 3B-D). As shown in Fig. 2C, GZ03639 expressing GCaMP5G exhibited comparable and consistent Ca^{2+} signatures to those observed in strains expressing YC3.60 (Fig. 3). Likewise, all mutants expressing GCaMP5G (Fig. 3B-D, black traces) showed pulsatile patterns (or lack thereof) consistent with their respective YC3.60 comparators (Fig. 3, red traces). Other subtle differences between pulsatile patterns for the various GCaMP5G or YC3.60 expressing strains were not discernable due to cell-to-cell variations commonly observed in time-lapse experiments. Overall, improvement in S/N with GCaMP5G relative to YC3.60 helped detect subtle oscillations in basal levels of $[Ca^{2+}]_c$.

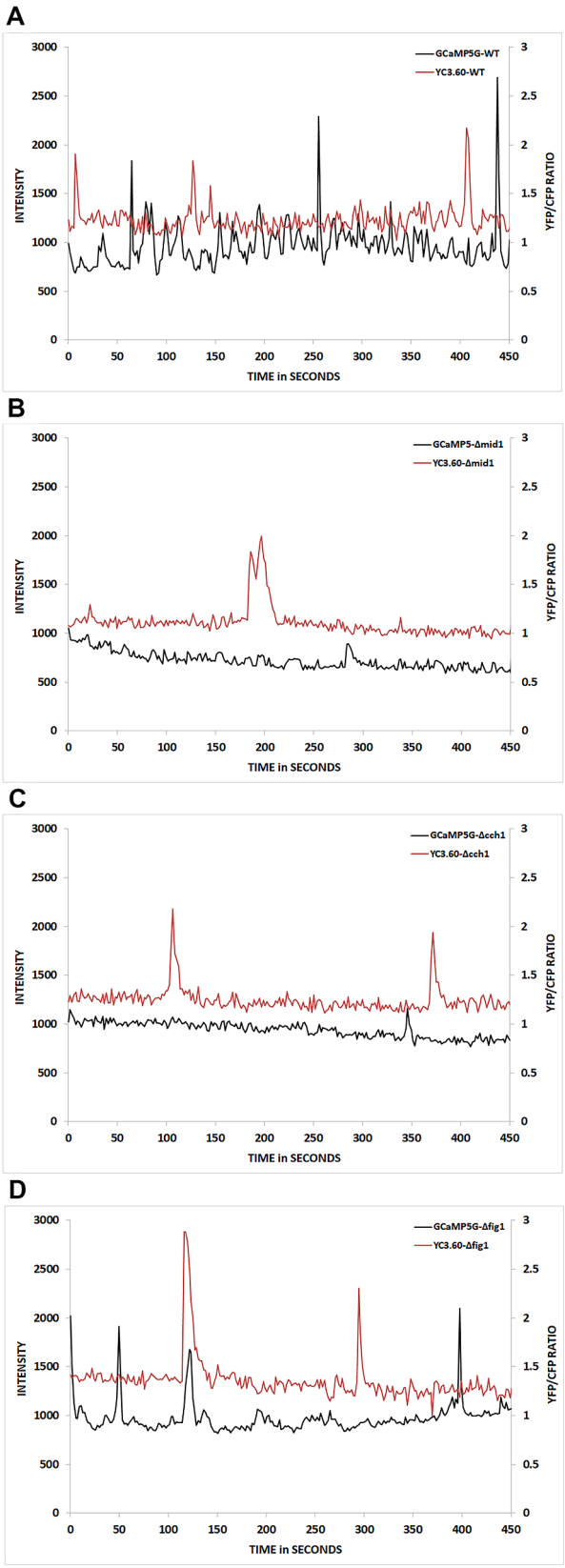

Fig. 3. (A) Comparison of Ca^{2+} signatures in *F. graminearum* strain GZ03639 and its Ca^{2+} channel mutants using GCaMP5G and YC3.60. Hyphal tips of GZ03639 (WT) expressing GCaMP5G, GZ03639 expressing YC3.60, and three mutants Δ*mid1*(B), Δ*cch1*(C), and Δ*fig1*(D) derived from both strains imaged after culturing them on Vogel agar containing 1 mM $CaCl_2$ for 2 days at 25 °C.

4. Discussion

Research on how Ca^{2+} signaling controls fungal growth, development, and pathogenesis had been hampered by the lack of a robust method for imaging spatial and temporal dynamics of subcellular Ca^{2+} until the successful expression of YC3.60 in *M. oryzae* and two *Fusarium* spp. (Kim et al., 2012). With YC3.60, Nakai et al. (2004) achieved a greater than 5-fold Ca^{2+}-dependent increase in the dynamic range of YFP/CFP ratio through a circular permutation of the bright YFP acceptor Venus. Stable expression of YC3.60 enabled imaging of Ca^{2+} signatures over extended periods *in vitro* and *in planta*, allowing the subcellular spatial and temporal dynamics of $[Ca^{2+}]_c$ to be elucidated in selected stages of the fungal life/disease cycle (Kim et al., 2012). Additionally, as hyphal tips are exquisitely sensitive to the addition of exogenous factors, monitoring Ca^{2+} signatures in response to different stimuli becomes less prone to artifacts caused by the application of Ca^{2+} indicators based on organic dyes. This Cameleon GECI also enabled inquiries about how disruption of critical genes involved in Ca^{2+} signaling affects the formation of Ca^{2+} signatures and how resulting changes in Ca^{2+} signatures correlate with phenotypic changes (Kim et al., 2018, 2015).

However, despite technical improvements and multiple advantages of YC3.60 over Ca^{2+} indicator dyes and new insights enabled by Ca^{2+} imaging via YC3.60, especially in combination with targeted gene disruption, it is not a panacea. Its characteristics presented some limitations depending on experimental requirements. First, because it consists of two intact FPs (CFP and YFP), it limits the spectral range and number of fluorophores that can be employed for multi-color experiments. Additionally, in cells expressing ratiometric GECIs, there is always a background signal, even in the absence of Ca^{2+}. YC3.60 has inherently reduced S/N due to the required mathematical signal image processing. Finally, the presence of two FPs as part of a fusion protein is more likely to cause artifacts due to steric hindrance compared to smaller single FP indicators.

Here, we sought to expand the toolbox available for fungal Ca^{2+} signaling research and circumvent some of the limitations of YC3.60 by seeking to express a variety of circularly permuted FP-based GECIs (Akerboom et al., 2013, 2012) in three fungi. The first reported application of GCaMP3 and GCaMP6f and subcellular imaging in a yeast system (Carbo et al., 2017) demonstrated $[Ca^{2+}]_c$ spikes during cell polarization that were dependent on pheromone concentration and the Mid1/Fig1 complex. Here, we sought to realize similar benefits of improved sensitivity and S/N of this collection of GECIs to facilitate future experiments involving the simultaneous imaging of multiple FP-fused proteins in filamentous fungi. We also evaluated multiple promoters to optimize their expression in different fungal species. GCaMP5G exhibited superior imaging and photophysical characteristics for studying Ca^{2+} signatures in *Fusarium* spp. GCaMP5G, driven by the RP27 gene promoter in *F. graminearum* and the EF1α gene promoter in *F. oxysporum*, had the most consistent and strong expression levels (Fig. 1A, B, I, J and movies). Although pRP27-YCaMP1a was also suitable for Ca^{2+} signature imaging (Figs. 1K, 1L, and 2), it exhibited low levels of photobleaching with continuous imaging for >5 min (Fig. 2A red trace). We also explored a matrix of other spectrally unique circular permuted GECIs (GCaMP3, BCaMP, CyCaMP, RCaMP) with various promoter combinations. While these variants were weakly expressed in some instances, many did not express at all (Supplementary Table 2). Unfortunately, in instances of weak expression, we deemed that these transformants were not suitable for routine monitoring or characterization of Ca^{2+} signatures, due to the poor S/N, decreased sensor sensitivity for capturing low level Ca^{2+} fluctuations, and the increased propensity to photobleaching (see Fig. 1M-N and 1O-P movies; Fig. 2B. blue trace).

It remains unknown why most GECIs failed to express or expressed only at very low levels in the evaluated fungal species/strains. We used co-transformation to screen a large number of GECIs under the control of multiple promoters quickly for expression in three species and confirmed the integration of introduced GECIs only for *F. graminearum* transformants. Although we screened 20–50 transformants of *F. oxysporum* and *N. carssa* with each construct, we cannot completely rule out the possibility that some GECI constructs were not inserted in all transformants. Since we did not check the copy number of inserted GECI constructs and where in the genome they were inserted, we do not know if the copy number or chromosomal context affected their expression. It is conceivable that kingdom/species-specific codon usage bias, which has been shown to impact both transcriptional and translational efficiency (Deng et al., 2020), could play a role. Codon optimization has proven indispensable for successfully expressing GFPs in fungal species that did not express the original mammalian optimized constructs, such as *N. crassa* (Zhoua et al., 2016), *Ustilago* (Roy and van Staden, 2019), and *Aspergillus* (Iriarte et al., 2012). Optimization of GECIs for expression in fungi via codon changes may allow their stable expression. The dim fluorescence of the early-generation blue, cyan, and yellow GECIs used here likely hampered our ability to see weak expression; newer, brighter variants could yield usable signals at similar expression levels.

It should be noted that the GECIs used in this study have all undergone extensive optimization in the time since our experiments began. The performance of GCaMP5G was improved first to the GCaMP6 variants (Akerboom et al., 2013; Chen et al., 2013) and then to jGCaMP7 (Dana et al., 2019). The RCaMP variants have been dramatically improved in terms of brightness and signal change, leading to jRCaMP1a and jRCaMP1b (Dana et al., 2016). A distinct red GECI, RGECO1 (Zhao et al., 2011), has undergone optimization to jRGECO1a (Dana et al., 2016). The original YCaMP sensors were quite dim and photolabile and had low signal change. The performance of this scaffold has been significantly increased with the jYCaMP indicators (Mohr et al., 2020). The blue BCaMP and cyan CyCaMP sensors perform quite poorly and have not yet been systematically optimized. Separate construction of a blue GECI led to B-GECO1 (Zhao et al., 2011), with similar performance to BCaMP. Other families of single-wavelength GECIs have also been developed based on other fluorescent proteins. The green NCaMP7 (Subach et al., 2020) and mNG-GECO1 (Zarowny et al., 2020) were based on mNeonGreen, the red K-GECO1 (Shen et al., 2018) from mKate, and the infrared NIR-GECO1 (Qian et al., 2019) based on mIFP, among others. Future experiments using these GECIs in filamentous fungi will be required to ensure that the performance enhancements seen in other systems help advance fungal Ca^{2+} signaling research. The improved GECI GCaMP6s has been successfully expressed in *Trichoderma atroviride* to investigate how Ca^{2+} signaling regulates a putative innate immune system during regeneration (Medina-Castellanos et al., 2018).

In combination with state-of-the-art imaging and gene manipulation tools, the expanding selection of GECIs will facilitate studies on the mechanism by which pulsatile $[Ca^{2+}]_c$ and other tip constituents (i.e., organelles, cytoskeleton, Ca^{2+} signaling proteins) control fungal hyphal tip growth and cellular responses to external stimuli. In particular, we are intrigued by new analogs of circular permutated GCaMP, which hold promise in compartmentalization of GECIs in mammalian organelles for simultaneous visualization of Ca^{2+} dynamics in the cytoplasm, mitochondria, and endoplasmic reticulum (ER) through an approach called Calcium-Measuring Organelle-entrapped Protein Indicators (CEPIA) (Suzuki et al., 2014). The CEPIA strategy exquisitely revealed temporal and spatial heterogeneity in Ca^{2+} dynamics between the cytoplasm and organelles, which should help investigate the precise origin of tip high gradients and pulsatile Ca^{2+} signatures. It is conceivable that tip high $[Ca^{2+}]_c$ oscillations are derived from storage organelles (ER, vacuoles, and mitochondria) immediately adjacent to the Spitzenkörper. It has been demonstrated that Ca^{2+} transients in polarized cells facilitate vesicle fusion (Hoffmann et al., 2019), including the Spitzenkörper (Takeshita et al., 2017). Indeed, in *Saccharomyces cerevisiae*, correlative cryo-electron tomography of cells showed elevated $[Ca^{2+}]_c$ using GCaMP6f facilitated membrane bending of the ER and its fusion to the plasma membrane. As has been shown in *S. cerevisiae*, we found that the specific improvements in GCaMP5G performance over YC3.60 make it a

more robust tool in evaluating a host of Ca^{2+} signaling-related cell phenomena in filamentous fungi. The improved S/N and multi-color experiment flexibility with these circular permutated non-ratiometric GECIs will facilitate future studies on the role of Ca^{2+} signatures and dynamics.

CRediT authorship contribution statement

Hye-Seon Kim: Performed imaging experiments, generated some of the GECI constructs tested and draft preparation. **Jung-Eun Kim:** Built most of the GECI constructs tested, generated and screened transformants, phenotype characterization of transformants, and draft reparation. **Aram Hwangbo and Hokyoung Son:** Generated and screened *F. graminearum* transformants with GECIs. **Jasper Akerboom and Loren L. Looger:** Provided GECI variants and guided their cloning for fungal expression. **Randall Duncan, Kirk J. Czymmek and Seogchan Kang:** Experimental design, writing, and editing.

Declaration of Competing Interest

The authors declare that they have no known competing financial interests or personal relationships that could have appeared to influence the work reported in this paper.

Acknowledgements

This work was mainly supported by a grant from the U.S. National Science Foundation (MCB-1051667). The USDA National Institute of Food & Agriculture and Federal Appropriations (Project PEN04655; Accession # 1016291) supported S. Kang.

Appendix A. Supplementary material

Supplementary data to this article can be found online at https://doi.org/10.1016/j.fgb.2021.103540.

References

Akerboom, J., Calderón, N.C., Tian, L., Wabnig, S., Prigge, M., Tolö, J., Gordus, A., Orger, M.B., Severi, K.E., Macklin, J.J., Patel, R., Pulver, S.R., Wardill, T.J., Fischer, E., Schüler, C., Chen, T.W., Sarkisyan, K.S., Marvin, J.S., Bargmann, C.I., Kim, D.S., Kügler, S., Lagnado, L., Hegemann, P., Gottschalk, A., Schreiter, E.R., Looger, L.L., 2013. Genetically encoded calcium indicators for multi-color neural activity imaging and combination with optogenetics. Front. Mol. Neurosci. 6, 1–29. https://doi.org/10.3389/fnmol.2013.00002.

Akerboom, J., Chen, T.W., Wardill, T.J., Tian, L., Marvin, J.S., Mutlu, S., Calderón, N.C., Esposti, F., Borghuis, B.G., Sun, X.R., Gordus, A., Orger, M.B., Portugues, R., Engert, F., Macklin, J.J., Filosa, A., Aggarwal, A., Kerr, R.A., Takagi, R., Kracun, S., Shigetomi, E., Khakh, B.S., Baier, H., Lagnado, L., Wang, S.S.H., Bargmann, C.I., Kimmel, B.E., Jayaraman, V., Svoboda, K., Kim, D.S., Schreiter, E.R., Looger, L.L., 2012. Optimization of a GCaMP calcium indicator for neural activity imaging. J. Neurosci. 32, 13819–13840. https://doi.org/10.1523/JNEUROSCI.2601-12.2012.

Baird, G.S., Zacharias, D.A., Tsien, R.Y., 1999. Circular permutation and receptor insertion within green fluorescent proteins. Proc. Natl. Acad. Sci. U. S. A. 96, 11241–11246. https://doi.org/10.1073/pnas.96.20.11241.

Berepiki, A., Lichius, A., Shoji, J.Y., Tilsner, J., Read, N.D., 2010. F-actin dynamics in Neurospora crassa. Eukaryot. Cell 9, 547–557. https://doi.org/10.1128/EC.00253-09.

Borst, J.W., Laptenok, S.P., Westphal, A.H., Kühnemuth, R., Hornen, H., Visser, N.V., Kalinin, S., Aker, J., Van Hoek, A., Seidel, C.A.M., Visser, A.J.W.G., 2008. Structural changes of yellow cameleon domains observed by quantitative FRET analysis and polarized fluorescence correlation spectroscopy. Biophys. J. 95, 5399–5411. https://doi.org/10.1529/biophysj.107.114587.

Bowden, R.L., Leslie, J.F., 1999. Sexual recombination in Gibberella zeae. Phytopathology 89, 182–188. https://doi.org/10.1094/PHYTO.1999.89.2.182.

Chen, S., Song, Y., Cao, J., Wang, G., Wei, H., Xu, X., Lu, L., 2010. Localization and function of calmodulin in live-cells of Aspergillus nidulans. Fungal Genet. Biol. 47, 268–278. https://doi.org/10.1016/j.fgb.2009.12.008.

Chen, T.W., Wardill, T.J., Sun, Y., Pulver, S.R., Renninger, S.L., Baohan, A., Schreiter, E. R., Kerr, R.A., Orger, M.B., Jayaraman, V., Looger, L.L., Svoboda, K., Kim, D.S., 2013. Ultrasensitive fluorescent proteins for imaging neuronal activity. Nature 499, 295–300. https://doi.org/10.1038/nature12354.

Clapham, D.E., 2007. Calcium signaling. Cell 131, 1047–1058. https://doi.org/10.1016/j.cell.2007.11.028.

Crichton, R.R., 2012. Calcium – cellular signalling. Biol. Inorg. Chem. 215–228 https://doi.org/10.1016/b978-0-444-53782-9.00011-5.

Dana, H., Mohar, B., Sun, Y., Narayan, S., Gordus, A., Hasseman, J.P., Tsegaye, G., Holt, G.T., Hu, A., Walpita, D., Patel, R., Macklin, J.J., Bargmann, C.I., Ahrens, M.B., Schreiter, E.R., Jayaraman, V., Looger, L.L., Svoboda, K., Kim, D.S., 2016. Sensitive red protein calcium indicators for imaging neural activity. Elife 5, 1–24. https://doi.org/10.7554/eLife.12727.

Dana, H., Sun, Y., Mohar, B., Hulse, B.K., Kerlin, A.M., Hasseman, J.P., Tsegaye, G., Tsang, A., Wong, A., Patel, R., Macklin, J.J., Chen, Y., Konnerth, A., Jayaraman, V., Looger, L.L., Schreiter, E.R., Svoboda, K., Kim, D.S., 2019. High-performance calcium sensors for imaging activity in neuronal populations and microcompartments. Nat. Methods 16, 649–657. https://doi.org/10.1038/s41592-019-0435-6.

Davis, R.H., de Serres, F.J., 1970. Metabolism of amino acids and amines Part A. Methods Enzymol. 17, 79–143. https://doi.org/10.1016/0076-6879(71)17168-6.

Demaurex, N., 2005. Calcium measurements in organelles with Ca2+-sensitive fluorescent proteins. Cell Calcium 38, 213–222. https://doi.org/10.1016/j.ceca.2005.06.026.

Deng, Y., De Lima Hedayioglu, F., Kalfon, J., Chu, D., Von Der Haar, T., 2020. Hidden patterns of codon usage bias across kingdoms. J. R. Soc. Interface 17. https://doi.org/10.1098/rsif.2019.0819.

Diegelmann, S., Fiala, A., Leibold, C., Spall, T., Buchner, E., 2002. Transgenic flies expressing the fluorescence calcium sensor cameleon 2.1 under UAS control. Genesis 34, 95–98. https://doi.org/10.1002/gene.10112.

Dodd, A.N., Kudla, J., Sanders, D., 2010. The language of calcium signaling. Annu. Rev. Plant Biol. 61, 593–620. https://doi.org/10.1146/annurev-arplant-070109-104628.

Galagan, J.E., Calvo, S.E., Borkovich, K.A., Selker, E.U., Read, N.O., Jaffe, D., FitzHugh, W., Ma, L.J., Smirnov, S., Purcell, S., Rehman, B., Elkins, T., Engels, R., Wang, S., Nielsen, C.B., Butler, J., Endrizzi, M., Qui, D., Ianakiev, P., Bell-Pedersen, D., Nelson, M.A., Werner-Washburne, M., Selitrennikoff, C.P., Kinsey, J.A., Braun, E.L., Zelter, A., Schulte, U., Kothe, G.O., Jedd, G., Mewes, W., Staben, C., Marcotte, E., Greenberg, D., Roy, A., Foley, K., Naylor, J., Stange-Thomann, N., Barrett, R., Gnerre, S., Kamal, M., Kamvysselis, M., Mauceli, E., Bielke, C., Rudd, S., Frishman, D., Krystofova, S., Rasmussen, C., Metzenberg, R.L., Perkins, D.D., Kroken, S., Cogoni, C., Macino, G., Catcheside, D., Li, W., Pratt, R.J., Osmani, S.A., DeSouza, C.P.C., Glass, L., Orbach, M.J., Berglund, J.A., Voelker, R., Yarden, O., Plamann, M., Seiler, S., Dunlap, J., Radford, A., Aramayo, R., Natvig, D.O., Alex, L. A., Mannhaupt, G., Ebbole, D.J., Freitag, M., Paulsen, I., Sachs, M.S., Lander, E.S., Nusbaum, C., Birren, B., 2003. The genome sequence of the filamentous fungus Neurospora crassa. Nature 422, 859–868. https://doi.org/10.1038/nature01554.

Grienberger, C., Konnerth, A., 2012. Imaging calcium in neurons. Neuron 73, 862–885. https://doi.org/10.1016/j.neuron.2012.02.011.

Hasan, M.T., Friedrich, R.W., Euler, T., Larkum, M.E., Giese, G., Both, M., Duebel, J., Waters, J., Bujard, H., Griesbeck, O., Tsien, R.Y., Nagai, T., Miyawaki, A., Denk, W., 2004. Functional fluorescent Ca2+ indicator proteins in transgenic mice under TET control. PLoS Biol. 2, 763–775. https://doi.org/10.1371/journal.pbio.0020163.

Hofer, A.M., Brown, E.M., 2003. Extracellular calcium sensing and signalling. Nat. Rev. Mol. Cell Biol. 4, 530–538.

Hoffmann, P.C., Bharat, T.A.M., Wozny, M.R., Boulanger, J., Miller, E.A., Kukulski, W., 2019. Tricalbins contribute to cellular lipid flux and form curved ER-PM contacts that are bridged by rod-shaped structures. Dev. Cell 51, 488–502.e8. https://doi.org/10.1016/j.devcel.2019.09.019.

Horikawa, K., Yamada, Y., Matsuda, T., Kobayashi, K., Hashimoto, M., Matsu-Ura, T., Miyawaki, A., Michikawa, T., Mikoshiba, K., Nagai, T., 2010. Spontaneous network activity visualized by ultrasensitive Ca^{2+} indicators, yellow Cameleon-Nano. Nat. Methods 7, 729–732. https://doi.org/10.1038/nmeth.1488.

Iriarte, A., Sanguinetti, M., Fernández-Calero, T., Naya, H., Ramón, A., Musto, H., 2012. Translational selection on codon usage in the genus Aspergillus. Gene 506, 98–105. https://doi.org/10.1016/j.gene.2012.06.027.

Kanchiswamy, C.N., Malnoy, M., Occhipinti, A., Maffei, M.E., 2014. Calcium imaging perspectives in plants. Int. J. Mol. Sci. 15, 3842–3859. https://doi.org/10.3390/ijms15033842.

Kim, H.-S., Czymmek, K.J., Patel, A., Modla, S., Nohe, A., Duncan, R., Gilroy, S., Kang, S., 2012. Expression of the Cameleon calcium biosensor in fungi reveals distinct Ca^{2+} signatures associated with polarized growth, development, and pathogenesis. Fungal Genet. Biol. 49 https://doi.org/10.1016/j.fgb.2012.05.011.

Kim, H.-S., Kim, J.-E., Frailey, D., Nohe, A., Duncan, R., Czymmek, K.J., Kang, S., 2015. Roles of three Fusarium oxysporum calcium ion (Ca^{2+}) channels in generating Ca^{2+} signatures and controlling growth. Fungal Genet. Biol. 82 https://doi.org/10.1016/j.fgb.2015.07.003.

Kim, H.-S., Kim, J.-E., Son, H., Frailey, D., Cirino, R., Lee, Y.-W., Duncan, R., Czymmek, K.J., Kang, S., 2018. Roles of three Fusarium graminearum membrane Ca^{2+} channels in the formation of Ca^{2+} signatures, growth, development, pathogenicity and mycotoxin production. Fungal Genet. Biol. 111 https://doi.org/10.1016/j.fgb.2017.11.005.

Knight, M.R., Campbell, A.K., Smith, S.M., Trewavas, A.J., 1991. Recombinant aequorin as a probe for cytosolic free Ca^{2+} in Escherichia coli. FEBS Lett. 282, 405–408. https://doi.org/10.1016/0014-5793(91)80524-7.

Kostyuk, A.I., Demidovich, A.D., Kotova, D.A., Belousov, V.V., Bilan, D.S., 2019. Circularly permuted fluorescent protein-based indicators: History, principles, and classification. Int. J. Mol. Sci. 20 https://doi.org/10.3390/ijms20174200.

Kotlikoff, M.I., 2007. Genetically encoded Ca^{2+} indicators: Using genetics and molecular design to understand complex physiology. J. Physiol. 578, 55–67. https://doi.org/10.1113/jphysiol.2006.120212.

Krebs, M., Held, K., Binder, A., Hashimoto, K., Den Herder, G., Parniske, M., Kudla, J., Schumacher, K., 2012. FRET-based genetically encoded sensors allow high-

resolution live cell imaging of Ca^{2+} dynamics. Plant J. 69, 181–192. https://doi.org/10.1111/j.1365-313X.2011.04780.x.

Lee, J., Son, H., Lee, S., Park, A.R., Lee, Y.-W., 2010. Development of a conditional gene expression system using a zearalenone-inducible promoter for the ascomycete fungus *Gibberella zeae*. Appl. Environ. Microbiol. 76, 3089–3096. https://doi.org/10.1128/AEM.02999-09.

Liu, S., He, J., Jin, H., Yang, F., Lu, J., Yang, J., 2011. Enhanced dynamic range in a genetically encoded Ca^{2+} sensor. Biochem. Biophys. Res. Commun. 412, 155–159. https://doi.org/10.1016/j.bbrc.2011.07.065.

Ma, L.J., Van Der Does, H.C., Borkovich, K.A., Coleman, J.J., Daboussi, M.J., Di Pietro, A., Dufresne, M., Freitag, M., Grabherr, M., Henrissat, B., Houterman, P.M., Kang, S., Shim, W.B., Woloshuk, C., Xie, X., Xu, J.R., Antoniw, J., Baker, S.E., Bluhm, B.H., Breakspear, A., Brown, D.W., Butchko, R.A.E., Chapman, S., Coulson, R., Coutinho, P.M., Danchin, E.G.J., Diener, A., Gale, L.R., Gardiner, D.M., Goff, S., Hammond-Kosack, K.E., Hilburn, K., Hua-Van, A., Jonkers, W., Kazan, K., Kodira, C.D., Koehrsen, M., Kumar, L., Lee, Y.H., Li, L., Manners, J.M., Miranda-Saavedra, D., Mukherjee, M., Park, G., Park, J., Park, S.Y., Proctor, R.H., Regev, A., Ruiz-Roldan, M.C., Sain, D., Sakthikumar, S., Sykes, S., Schwartz, D.C., Turgeon, B. G., Wapinski, I., Yoder, O., Young, S., Zeng, Q., Zhou, S., Galagan, J., Cuomo, C.A., Kistler, H.C., Rep, M., 2010. Comparative genomics reveals mobile pathogenicity chromosomes in Fusarium. Nature 464, 367–373. https://doi.org/10.1038/nature08850.

Martin, J.R., Rogers, K.L., Chagneau, C., Brûlet, P., 2007. In vivo bioluminescence imaging of Ca^{2+} signalling in brain of Drosophila. PLoS ONE 2, 2–9. https://doi.org/10.1371/journal.pone.0000275.

McAinsh, M.R., Pittman, J.K., 2009. Shaping the calcium signature. New Phytol. 181, 275–294. https://doi.org/10.1111/j.1469-8137.2008.02682.x.

McCombs, J.E., Palmer, A.E., 2008. Measuring calcium dynamics in living cells with genetically encodable calcium indicators. Methods 46, 152–159. https://doi.org/10.1016/j.ymeth.2008.09.015.

Medina-Castellanos, E., Villalobos-Escobedo, J.M., Riquelme, M., Read, N.D., Abreu-Goodger, C., Herrera-Estrella, A., 2018. Danger signals activate a putative innate immune system during regeneration in a filamentous fungus. PLoS Genet. 14, 1–15. https://doi.org/10.1371/journal.pgen.1007390.

Miwa, H., Sun, J., Oldroyd, G.E.D., Allan Downie, J., 2006. Analysis of calcium spiking using a cameleon calcium sensor reveals that nodulation gene expression is regulated by calcium spike number and the developmental status of the cell. Plant J. 48, 883–894. https://doi.org/10.1111/j.1365-313X.2006.02926.x.

Mohr, M.A., Bushey, D., Aggarwal, A., Marvin, J.S., Kim, J.J., Marquez, E.J., Liang, Y., Patel, R., Macklin, J.J., Lee, C.-Y., Tsang, A., Tsegaye, G., Ahrens, A.M., Chen, J.L., Kim, D.S., Wong, A.M., Looger, L.L., Schreiter, E.R., Podgorski, K., 2020. jYCaMP: an optimized calcium indicator for two-photon imaging at fiber laser wavelengths. Nat. Methods 17, 694–697. https://doi.org/10.1038/s41592-020-0835-7.

Monshausen, G.B., Messerli, M.A., Gilroy, S., 2008. Imaging of the Yellow Cameleon 3.6 indicator reveals that elevations in cytosolic Ca^{2}+ follow oscillating increases in growth in root hairs of Arabidopsis. Plant Physiol. 147, 1690–1698. https://doi.org/10.1104/pp.108.123638.

Nagai, T., Yamada, S., Tominaga, T., Ichikawa, M., Miyawaki, A., 2004. Expanded dynamic range of fluorescent indicators for Ca^{2+} by circularly permuted yellow fluorescent proteins. Proc. Natl. Acad. Sci. U. S. A. 101, 10554–10559. https://doi.org/10.1073/pnas.0400417101.

Nair, R., Raina, S., Keshavarz, T., Kerrigan, M.J.P., 2011. Application of fluorescent indicators to analyse intracellular calcium and morphology in filamentous fungi. Fungal Biol. 115, 326–334. https://doi.org/10.1016/j.funbio.2010.12.012.

Nakai, J., Ohkura, M., Imoto, K., 2001. A high signal-to-noise Ca^{2+} probe composed of a single green fluorescent protein. Nat. Biotechnol. 19, 137–141. https://doi.org/10.1038/84397.

Nelson, G., Kozlova-Zwinderman, O., Collis, A.J., Knight, M.R., Fincham, J.R.S., Stanger, C.P., Renwick, A., Hessing, J.G.M., Punt, P.J., Van Den Hondel, C.A.M.J.J., Read, N.D., 2004. Calcium measurements in living filamentous fungi expressing codon-optimized aequorin. Mol. Microbiol. 52, 1437–1450. https://doi.org/10.1111/j.1365-2958.2004.04066.x.

Ohkura, M., Matsuzaki, M., Kasai, H., Imoto, K., Nakai, J., 2005. Genetically encoded bright Ca^{2+} probe applicable for dynamic Ca^{2+} imaging of dendritic spines. Anal. Chem. 77, 5861–5869. https://doi.org/10.1021/ac0506837.

Paredes, R.M., Etzler, J.C., Watts, L.T., Zheng, W., Lechleiter, J.D., 2008. Chemical calcium indicators. Methods 46, 143–151. https://doi.org/10.1016/j.ymeth.2008.09.025.

Qian, Y., Piatkevich, K.D., Mc Larney, B., Abdelfattah, A.S., Mehta, S., Murdock, M.H., Gottschalk, S., Molina, R.S., Zhang, W., Chen, Y., Wu, J., Drobizhev, M., Hughes, T. E., Zhang, J., Schreiter, E.R., Shoham, S., Razansky, D., Boyden, E.S., Campbell, R.E., 2019. A genetically encoded near-infrared fluorescent calcium ion indicator. Nat. Methods 16, 171–174. https://doi.org/10.1038/s41592-018-0294-6.

Rincón-Zachary, M., Teaster, N.D., Alan Sparks, J., Valster, A.H., Motes, C.M., Blancaflor, E.B., 2010. Fluorescence resonance energy transfer-sensitized emission of yellow cameleon 3.60 reveals root zone-specific calcium signatures in Arabidopsis in response to aluminum and other trivalent cations. Plant Physiol. 152, 1442–1458. https://doi.org/10.1104/pp.109.147256.

Roy, A., van Staden, J., 2019. Comprehensive profiling of codon usage signatures and codon context variations in the genus Ustilago. World J. Microbiol. Biotechnol. 35, 1–15. https://doi.org/10.1007/s11274-019-2693-y.

Rudolf, R., Mongillo, M., Magalhães, P.J., Pozzan, T., 2004. In vivo monitoring of Ca^{2+} uptake into mitochondria of mouse skeletal muscle during contraction. J. Cell Biol. 166, 527–536. https://doi.org/10.1083/jcb.200403102.

Shen, Y., Dana, H., Abdelfattah, A.S., Patel, R., Shea, J., Molina, R.S., Rawal, B., Rancic, V., Chang, Y.F., Wu, L., Chen, Y., Qian, Y., Wiens, M.D., Hambleton, N., Ballanyi, K., Hughes, T.E., Drobizhev, M., Kim, D.S., Koyama, M., Schreiter, E.R., Campbell, R.E., 2018. A genetically encoded Ca^{2+} indicator based on circularly permutated sea anemone red fluorescent protein eqFP578. BMC Biol. 16, 1–16. https://doi.org/10.1186/s12915-018-0480-0.

Silverman-Gavrila, L.B., Lew, R.R., 2003. Calcium gradient dependence of Neurospora crassa hyphal growth. Microbiology 149, 2475–2485. https://doi.org/10.1099/mic.0.26302-0.

Slusarski, D.C., Pelegri, F., 2007. Calcium signaling in vertebrate embryonic patterning and morphogenesis. Dev. Biol. 307, 1–13. https://doi.org/10.1016/j.ydbio.2007.04.043.

Son, H., Lee, J., Park, A.R., Lee, Y.-W., 2011. ATP citrate lyase is required for normal sexual and asexual development in *Gibberella zeae*. Fungal Genet. Biol. 48, 408–417.

Steinhorst, L., Kudla, J., 2014. Signaling in cells and organisms - calcium holds the line. Curr. Opin. Plant Biol. 22, 14–21. https://doi.org/10.1016/j.pbi.2014.08.003.

Subach, O.M., Sotskov, V.P., Plusnin, V.V., Gruzdeva, A.M., Barykina, N.V., Ivashkina, O. I., Anokhin, K.V., Nikolaeva, A.Y., Korzhenevskiy, D.A., Vlaskina, A.V., Lazarenko, V.A., Boyko, K.M., Rakitina, T.V., Varizhuk, A.M., Pozmogova, G.E., Podgorny, O.V., Piatkevich, K.D., Boyden, E.S., Subach, F.V., 2020. Novel genetically encoded bright positive calcium indicator ncamp7 based on the mneongreen fluorescent protein. Int. J. Mol. Sci. 21, 1–24. https://doi.org/10.3390/ijms21051644.

Suzuki, J., Kanemaru, K., Ishii, K., Ohkura, M., Okubo, Y., Iino, M., 2014. Imaging intraorganellar Ca^{2+} at subcellular resolution using CEPIA. Nat. Commun. 5, 1–13. https://doi.org/10.1038/ncomms5153.

Takahashi, A., Camacho, P., Lechleiter, J.D., Herman, B., 1999. Measurement of intracellular calcium. Physiol. Rev. 79, 1089–1125. https://doi.org/10.1152/physrev.1999.79.4.1089.

Takeshita, N., Evangelinos, M., Zhou, L., Serizawa, T., Somera-Fajardo, R.A., Lu, L., Takaya, N., Nienhaus, G.U., Fischer, R., 2017. Pulses of Ca^{2+} coordinate actin assembly and exocytosis for stepwise cell extension. Proc. Natl. Acad. Sci. U. S. A. 114, 5701–5706. https://doi.org/10.1073/pnas.1700204114.

Thomas, D., Tovey, S.C., Collins, T.J., Bootman, M.D., Berridge, M.J., Lipp, P., 2000. A comparison of fluorescent Ca2+ indicator properties and their use in measuring elementary and global Ca^{2+} signals. Cell Calcium 28, 213–223. https://doi.org/10.1054/ceca.2000.0152.

Tian, L., Hires, S.A., Mao, T., Huber, D., Chiappe, M.E., Chalasani, S.H., Petreanu, L., Akerboom, J., McKinney, S.A., Schreiter, E.R., Bargmann, C.I., Jayaraman, V., Svoboda, K., Looger, L.L., 2009. Imaging neural activity in worms, flies and mice with improved GCaMP calcium indicators. Nat. Methods 6, 875–881. https://doi.org/10.1038/nmeth.1398.

Wang, G., Lu, L., Zhang, C.Y., Singapuri, A., Yuan, S., 2006. Calmodulin concentrates at the apex of growing hyphae and localizes to the Spitzenkörper in Aspergillus nidulans. Protoplasma 228, 159–166. https://doi.org/10.1007/s00709-006-0181-3.

Watahiki, M.K., Trewavas, A.J., Parton, R.M., 2004. Fluctuations in the pollen tube tip-focused calcium gradient are not reflected in nuclear calcium level: A comparative analysis using recombinant yellow cameleon calcium reporter. Sex. Plant Reprod. 17, 125–130. https://doi.org/10.1007/s00497-004-0224-x.

Zarowny, L., Aggarwal, A., Rutten, V.M.S., Kolb, I., Patel, R., Huang, H.-Y., Chang, Y.-F., Phan, T., Kanyo, R., Ahrens, M.B., Allison, W.T., Podgorski, K., Campbell, R.E., 2020. Bright and high-performance genetically encoded Ca^{2+} indicator based on mNeonGreen fluorescent protein. ACS Sensors 5, 1959–1968. https://doi.org/10.1021/acssensors.0c00279.

Zhao, Y., Araki, S., Wu, J., Teramoto, T., Chang, Y.-F., Nakano, M., Abdelfattah, A.S., Fujiwara, M., Ishihara, T., Nagai, T., Campbell, R.E., 2011. An expanded palette of genetically encoded Ca^{2+} indicators. Science 333, 1888–1891. https://doi.org/10.1126/science.1208592.

Zhoua, Z., Danga, Y., Zhou, M., Li, L., Yu, C.H., Fu, J., Chen, S., Liu, Y., 2016. Codon usage is an important determinant of gene expression levels largely through its effects on transcription. Proc. Natl. Acad. Sci. U. S. A. 113, E6117–E6125. https://doi.org/10.1073/pnas.1606724113.